Tank-Like Module-Based Climbing Robot Using Passive Compliant Joints

TaeWon Seo, *Member, IEEE*, and Metin Sitti, *Senior Member, IEEE*

Abstract—This paper proposes an underactuated modular climbing robot with flat dry elastomer adhesives. This robot is designed to achieve high speed, high payload, and dexterous motions that are typical drawbacks of previous climbing robots. Each module is designed as a tread-wheeled mechanism to simultaneously realize high speed and high adhesive force. Two modules are connected by compliant joints, which induce a positive preload on the front wheels resulting in stable climbing and high payload capacity. Compliant joints also help the robot to perform various transitions. An active tail is adopted to regulate the preload of the second module. Force transfer equations are derived and stable operating conditions are verified. The stiffness coefficients of the compliant joints and the active tail force are determined optimally to satisfy the constraints of stable operation. The prototype two-module robot achieves 6-cm/s speed and 500-g payload capacity on vertical surfaces. The abilities of flat surface locomotion, internal, external, and thin-wall transitions, and overcoming various sized obstacles are validated through experiment. The principle of joint compliance can be adopted in other climbing robots to enhance their stability and transition capability.

Index Terms—Active tail, climbing robot, directional compliant joint, flat elastomer adhesive, overcoming obstacle, transition.

I. INTRODUCTION

CLIMBING robots have been developed to be applied in hazardous and dangerous environments for human beings like exploring [1], inspecting [2], [3], and cleaning of high-rise buildings [4]. Since climbing on a vertical wall or on a ceiling works against the direction of gravity, sufficient attachment force (shear resistance and adhesion) is required for climbing robots to maintain their position on the vertical wall. There are several principles to make this attachment force: suction [5], magnetic force [6], mechanical interlocking [7], vortex [8], and electroadhesives [9]. However, each of these has a drawback

such as limited surface choice (in the case of magnetic forces, mechanical interlocking, and electroadhesives) and power consumption (in the case of suction and vortex). Recently, dry adhesive materials of flat or fibrillar structures have been proposed due to their advantage of attachment to various surfaces with low power consumption [10], [11]. Recent research on such dry adhesives focus on preventing contamination using self-cleaning abilities [12].

Some climbing robots using flat or fibrillar dry adhesive materials have been introduced from bioinspiration [13]. Stickybot was developed for upward climbing using directional fibrillar footpads and hierarchical complaint body design [14]. Mini-Whegs was proposed, which used sticky tape as an attaching unit with a unique wheel design combining advantages of wheels and legs [15]. Waalbot was developed with mushroom-shaped microfibers and rotating compliant legs composed of three footpads with fibers [16]. Geckobot was developed with a flat elastomer adhesive and a four-legged body design [11]. Even though these robots successfully validated their performance in basic experimental conditions, there are some remaining issues to be improved such as preload and climbing speed. Capabilities of internal and external transitioning, and obstacle overcoming also need to be improved.

Recently, Tankbot that adopts flat elastomer treads and an active tail was proposed by Unver and Sitti [17], [18]. This robot is designed as a wheeled mechanism to achieve high-speed climbing (12 cm/s) on a vertical surface. By using flexible treads and an active tail, this robot has abilities of transitioning, overcoming obstacles, steering, and inverted climbing. Even though Tankbot shows abilities of relatively dexterous and maneuverable motions, the robot can only perform limited transitions (two internal transitions and one external transition). Moreover, the robot cannot perform large obstacle overcoming and thin-wall transitioning, which can be defined by wall-to-wall transitioning that changes the direction of movement in 180° (e.g., vertical upward to vertical downward transitioning). Payload capacity also needs to be improved for various tasks.

Compliance design is one of the important issues in mobile robot design to make robots adapt to unexpected environmental conditions [19]. Stickybot is designed as a flexible mechanism using a hierarchical compliance structure from its footpad to main body [14]. The hexapedal robot DASH, inspired by the cockroach, is manufactured from flexible cardboard, and the robot can climb steps due to its high level of compliance [20]. Spinybot uses spiny footpads that adopt using the mechanical interlocking attaching principle, and the probability of successful attachment is increased by the compliant microspine arrays [21]. Previous research shows that compliance can help

TABLE I
DESIGN REQUIREMENTS AND THE PERFORMANCE OF EXISTING CLIMBING ROBOT USING FLAT OR PATTERNED POLYMER ADHESIVES

	Stickybot	Geckobot	Waalbot	Mini-Whegs	Tankbot	Proposed robot
Speed (mm/sec)	40	10	60	58	120	≥ 60
Roughness	Smooth	Smooth/rough	Smooth	Smooth/rough	Smooth/rough	Smooth/rough
Transition	No	No	3 int./ 0 ext.	4 int./ 0 ext.	3 int./ 1 ext.	As many as possible
Obstacles (mm)	No	No	No	≤ 11.1	≤ 15	≥ 22 (wheel size)
Thin-wall	No	No	No	No	No	Yes
Inverted climbing	No	Yes	No	Yes	Yes	Yes
Payload (g)	N/A	25	N/A	N/A	100	≥ 300
Steering	No	No	Yes	Yes	No	No

robots adapt to uneven environmental conditions. Our research using directional compliances builds on a simple idea: the directional compliance can regulate the preload toward the attachment surface to increase climbing stability. Additionally, the directional compliance also enables the robot to transition and overcome obstacles passively.

This paper aims to develop a stable climbing robot that is able to climb on various angled surfaces with high payload, transitioning, and obstacle-overcoming capabilities. Modular design is adopted due to its advantages of high mobility for dexterous motions. A wheeled mechanism using flexible treads and flat dry elastomers proposed in Tankbot is used to achieve high speed and high payload carrying capacity. Compliant body joints are used to enhance the stability by regulating preloads and to adapt to surface conditions by changing joint angles between each module according to external constraining conditions. As a result, the robot can perform various internal, external, and thin-wall transitions and can overcome relatively large obstacles passively. Since the passive directional compliant joint angles are changed automatically according to external constraining conditions, a complex control algorithm is not required. Instead, a relatively simple controller is used to achieve various motions.

The paper is organized as follows. Section II defines the design requirements and explains the configuration of the proposed climbing robot. Section III conducts force analysis of flat surface climbing, including preload calculation and surface normal force calculation. Design parameters (DPs) of the climbing robot are determined in Section IV to guarantee stable climbing while satisfying the constraints of various transitions. Section V presents experimental results and discussions on flat surface climbing, transitioning, and overcoming obstacles. Finally, concluding remarks are presented in Section VI.

II. DESIGN OF MODULAR CLIMBING ROBOT

A. Requirements for Design

Brief specifications of requirements are summarized in Table I, and comparable specifications of other robots from the literature are also presented. As shown in Table I, the objective of the design is to develop a high-speed climbing robot that is able to perform various tasks. Specifically, this research tries to design a robot to achieve stable internal, external, and thin-wall transitioning and relatively large obstacle overcoming tasks that are very critical moving conditions for climbing robots. Steering is not considered in the proposed climbing robot, but skid-steering with limited radius of curvature via independent speed control of left-right wheels as [17] can be used to steer it

TABLE II
IMPORTANT PARAMETERS FOR THE ANALYSIS

Parameters related to forces and torques	
^iF_f	preloads on the front wheel of ith module
^iF_r	preloads on the rear wheel of ith module
F_p	peeling force at the rear wheel
F_s	slack force of the tread
F_t	active tail force at the end of the tail
^iN	normal force of the tread of ith module
k_i	stiffness coefficient of the ith compliant joint
φ_i	rotation angle of the ith compliant joint
σ_a	V-10 elastomer adhesion pressure
τ	V-10 elastomer shear strength
Parameters related to geometry	
L_f	distance between the front wheel and the center of gravity (CG)
L_r	distance between CG and the rear wheel
L_c	length of the connecting link
L_t	length of the active tail
r_w	radius of the wheel
h_{CG}	height from the attaching surface to CG
m_i	mass of i_{th} module
A_c	contact area of the tread

as a future work. Detailed design specifications are introduced in Section II, and the performances is empirically validated in Section V.

B. Robot Configuration

Modular robot systems are widely researched because of their advantages in versatility, robustness, and manufacturing costs [22]. Several researchers have proposed modular climbing robots using active rotating joints for transitioning and overcoming obstacles [8], [23]. However, due to the design complexity of modular climbing robots, control and motion planning are significant challenges.

The design of the proposed two-module climbing robot is shown in Fig. 1. Important parameters for the analysis are summarized in Table II. Each module is designed as a tread-wheeled mechanism. The tread-wheel mechanism has an advantage of high speed and stability [24], [25]. The first and second modules are connected by left and right links that consist of four compliant joints. Red solid arrows denote the direction of compliant torques. Note that stiffness of each compliant joint is different in order to efficiently increase the preload on each front wheel. The second module contains an active tail as shown in Fig. 1.

Each module is designed to use a tread of Vytaflex-10 (V-10, Smooth-on Inc.) elastomer. The V-10 elastomer is successfully validated as an adhesive material on various rough surfaces in the previous research [11], [26]. Detailed specifications of V-10 elastomer as adhesive is summarized in Section III-A. Since the adhesion force of V-10 elastomer is proportional to contact area, the adhesion force can be extensively increased by designing the wheel as a tread shape, increasing area contact. Compliance of

This article has been accepted for inclusion in a future issue of this journal. Content is final as presented, with the exception of pagination.

SEO AND SITTI: TANK-LIKE MODULE-BASED CLIMBING ROBOT USING PASSIVE COMPLIANT JOINTS
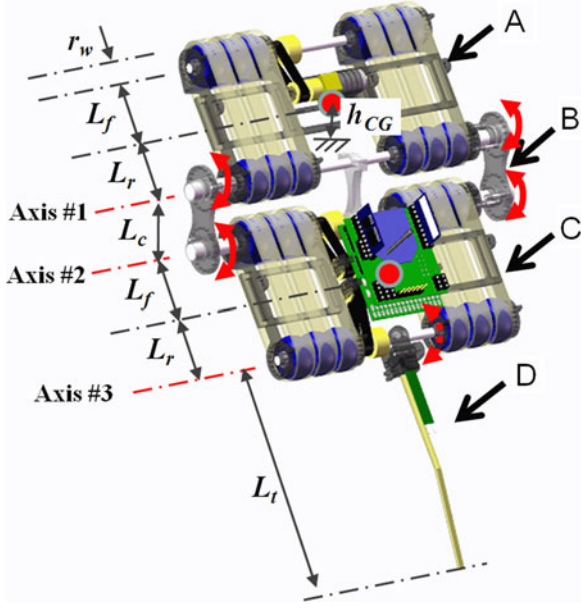
3

Fig. 1. Configuration of the modular climbing robot: A denotes the first module including tread-wheel and actuator; B denotes the connecting links with two compliant joints (solid red arrows denote directions of the compliant torques of joint); C denotes the second module including control board, wheel-tread, and actuators; and D denotes the active tail with force sensor (dotted red arrow denotes the direction of the active tail torque).

the tread is also helpful to adapt to uneven environments during transitioning and when overcoming obstacles. The tread was manufactured by a laser cutter after molding the V-10 polymer in a petri dish. The adhesive force, which is a function of the contact area, might be improved by widening the track width or adding more wheels in parallel; however, there are problems in manufacturing uniform treads with precise alignment.

The tread-wheel module is composed of two wheels and a V-10 tread. We designed the two-wheel mechanism instead of inserting rollers between the two wheels [25]. From simulations and experiments, the rollers between the wheels are proven not to be helpful to increase the climbing stability of the tread-wheel mechanism since the pitch-back moment is increased. Also, the compliance of the tread between wheels affects internal and external transitions positively.

The connection between each module is designed as a passive compliant joint and an active tail is attached to the end of the second module, which is one of main characteristics of the proposed robot system. We can expect three positive effects of the design as following. First, the pitch-back moment that makes the climbing robot fall could be compensated. Research on Tankbot shows an effect of the active tail to reduce pitch-back moment, and this study shows that the pitch-back moment is successfully compensated using a combination of the passive joints and the active tail. Second, the compliant torque and the active tail torque create positive preload on the front wheel, and are an essential for stable climbing of the tread mechanism. After the tread of the front wheels are attached on the surface, the other parts of the treads are continuously attached to the surface via the tread mechanism. Third, the compliance and active tail

help the robot to perform external transitioning and overcome a thin-wall and obstacles without a complex controller. Since the direction of the compliance torque and the active tail torque are toward the surface as denoted by solid red arrows in Fig. 1, the robot can locomote on various shaped surfaces passively without feedback control. The compliant joint force also helps to stabilize locomotion in opposite rotations of red arrows along to the axis 1, 2, and 3 in Fig. 1 (e.g., internal transition) via increasing preload on the front wheels. In this case, the DPs of the compliant joints and active tail must be accurately designed to satisfy force constraints to realize these transitions and obstacle overcoming. Design of the compliance and the tail force is presented in Section IV.

III. FORCE ANALYSIS

A. Flat Dry Elastomer Adhesive

As mentioned in Section II, V-10 dry elastomer is adopted as the material of the adhesive tread for the climbing robot. V-10 elastomer has successfully proven itself as an adhesive material on smooth and rough surfaces. Characteristics of V-10 elastomer adhesive are clearly defined in previous research [11], and the required characteristics for climbing robot design are summarized in this section.

Adhesion force is the most important characteristic to determine the stability of a climbing robot. Theoretical adhesion strength σ_a, which is the vertical pull-off strength of the adhesive tread on the surface, is calculated as 2.16 kPa when the thickness of elastomer is much larger than footpad radius, and 100 kPa when the thickness is much smaller than footpad radius [27]. Therefore, the real adhesion strength of elastomer is known to be between 2.16 and 100 kPa. In failure analysis, the minimum adhesion strength of 2.16 kPa is used to calculate a robust margin of error for the climbing robot. This adhesion strength is also empirically verified, and the relation of the preload pressure of σ_p and the adhesion strength is defined as follows [11]:

$$\sigma_a = A\sigma_p^B \qquad (1)$$

where A and B are estimated as 9.86 and 0.269 from empirical data, respectively. Note that σ_p is defined as the vertical compressive stress on the elastomer tread. This experimental result also guarantees that the adhesion force stays between 2.16 and 100 kPa.

The tangential friction force f is also very important to prevent slipping during vertical climbing. Friction of V-10 elastomer is defined as follows [28]:

$$f = \mu N_L + \tau A_c \qquad (2)$$

where μ is the static-friction coefficient, N_L is the compressive normal force, τ is the elastomer shear strength, and A_c is the contact area. Note that in (2), the first component is the real standard load-based friction and the second component is the shear force due to an elastic deformation of the elastomer. From previous research, coefficients μ and τ are measured as 2 and 0.125 kPa, respectively [11].

Since the tread is peeled at the rear wheel, the peeling force affects the preload on the rear wheel. This peeling force pulls each

This article has been accepted for inclusion in a future issue of this journal. Content is final as presented, with the exception of pagination.

4

IEEE/ASME TRANSACTIONS ON MECHATRONICS

module toward attaching surface when the front wheels contact the surface. Also, smooth peeling due to the tread mechanism reduces vibrations and helps to make the robot stable. The peeling force F_p that is a function of peeling angle θ can be calculated as follows [29]:

$$\left(\frac{F_p}{w}\right)^2 \frac{1}{2tE} + \left(\frac{F_p}{w}\right)(1 - \cos\theta) - R = 0 \tag{3}$$

where w is the width of tread, t is the thickness of the elastomer, E is Young's modulus of V-10, θ is the angle between surface and peeled tread, and R is the adhesive energy of the elastomer. E and R are empirically measured as 110 kPa and 70 N/m, respectively [26]. θ is determined according to initial pretention that is related to an initial tread length and a tread length after assembly. This desired pretension is determined to maximize the peeling force on the rear wheel.

B. Force Transfer Relations

Adhesion force is maximized during operation of the sticky tread wheel, since the tread is propagated from the front wheel to the rear wheel and it makes the whole area of the tread come into contact. Therefore, a positive preload on the front wheel is essential to make the force propagation occur. From this, the preload on the wheels are clearly defined.

The preload on the wheels that is shown in Fig. 2 is determined by a summation of the five components induced by the gravity force ($^iF_{gf}, {}^iF_{gr}$), motor torque ($^iF_{mf}, {}^iF_{mr}$), compliant joint torque ($^iF_{cf}, {}^iF_{cr}$), peeling force ($^iF_{pr}$), and active tail torque ($^NF_{tf}, {}^NF_{tr}$) as follows:

$$^iF_f = {}^iF_{gf} + {}^iF_{mf} + {}^iF_{cf} + ({}^2F_{tf})$$
$$^iF_r = {}^iF_{gr} + {}^iF_{mr} + {}^iF_{cr} + {}^iF_{pr} + ({}^2F_{tr}) \tag{4}$$

where superscript $i = 1, 2$ denotes the preload of the ith module. The last subscripts f and r denote whether the preload acts on the front or the rear wheel, respectively. The last term induced by the active tail affects only the preload of the second module.

Each component of (4) is calculated as follows:

$$^iF_{gf} = m_i g\left(\frac{L_r \cos\alpha_i - h_{\mathrm{CG}} \sin\alpha_i}{L_f + L_r}\right) \tag{5}$$

$$^iF_{gr} = m_i g\left(\frac{L_f \cos\alpha_i + h_{\mathrm{CG}} \sin\alpha_i}{L_f + L_r}\right)$$

$$^iF_{mf} = -{}^iF_{mr} = -\frac{(F_p - F_s)r_w}{L_f + L_r} \tag{6}$$

$$^iF_{pr} = F_p \sin\theta \tag{7}$$

$$^2F_{tf} = F_t\left(\frac{L_t}{L_f + L_r}\right)$$

$$^2F_{tr} = -F_t\left(1 + \frac{L_t}{L_f + L_r}\right) \tag{8}$$

where L_f is the distance between the front wheel and the center of gravity (CG), L_r is the distance between CG and the rear wheel, r_w is the radius of the wheel, L_t is the length of the tail, h_{CG} is height from the attaching surface to CG, α_i is the surface slope of the ith module, m_i is mass of each module, and g is the
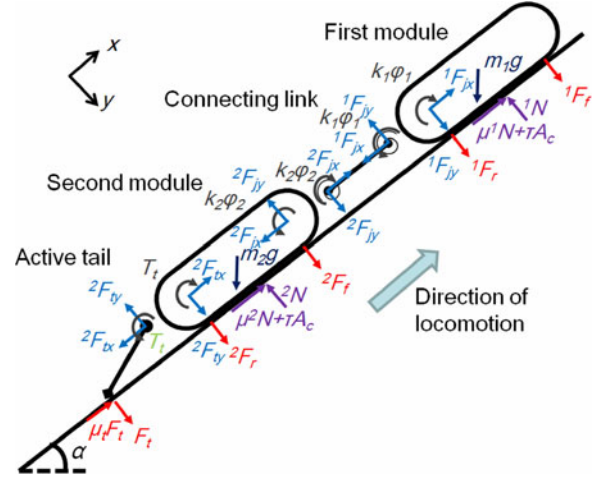

Fig. 2. Free-body diagram to calculate normal and joint reaction forces: ($^iF_{jx}, {}^iF_{jy}$) and ($^2F_{tx}, {}^2F_{ty}$) denote the reaction forces at the joint and the tail, respectively. T_t, μ_t, and F_t denote active tail torque, tail friction coefficient, and active tail reaction force, respectively.

gravitational acceleration. F_s is the slack force determined from the pretension and peeling forces as $F_s = 2wtE\epsilon - F_p$ where ϵ is an initial strain of the tread. F_t is the reaction force generated by the active tail.

The preload generated due to the compliant torque can be derived as follows:

$$^1F_{cf} = \frac{k_1\varphi_1}{L_f + L_r}$$

$$^1F_{cr} = -\frac{k_1\varphi_1}{L_f + L_r} - \frac{2(k_1\varphi_1 - k_2\varphi_2)}{L_c}$$

$$^2F_{cf} = -\frac{k_2\varphi_2}{L_f + L_r} + \frac{2(k_1\varphi_1 - k_2\varphi_2)}{L_c}$$

$$^2F_{cr} = \frac{k_2\varphi_2}{L_f + L_r} \tag{9}$$

where k_i and φ_i are the stiffness coefficient and the rotation angle of compliant joints of the ith modules, respectively. Note that φ_i is preloaded with $\pi/2$ in a flat configuration. L_c denotes the length of the connecting links. From (9), the preloads induced by the compliant joints always have a positive effect on the front wheel of the first module but could affect the front wheel of the second module negatively. This negative effect can be compensated by the positive force induced by the active tail in (8). The preload induced by gravity denoted in (5) changes according to α_i and sometimes causes the preload on the front wheel to be in the negative y-direction. Also, the preload induced by the motor torque in (6) have a negative effect on the preload of the front wheel. These negative effects on the preload of the front wheels might cause the robot to fail to operate stably. This negative effect can be compensated by varying the preloads induced by the compliant joints and active tail shown in (9) and (8) to make the preload on the front wheels positive for stable operation. This will be proved in Section III.

C. Surface Normal Forces

The surface normal force is directly related to the friction force as shown in (2), which is very important to prevent slipping of the climbing robot. For each module, the surface normal force can be calculated sequentially from the reaction forces on the compliant joint.

The free-body diagram to calculate the surface normal force is shown in Fig. 2. The surface normal force ^iN is assumed to be a point force normal to the CG. The normal forces can be calculated from the moment equilibrium equations of each module as follows:

$$^1N = \frac{^1F_f(L_f + L_r) + k_1\varphi_1 + m_1gL_r\cos\alpha_1 - \tau A_c h_{CG}}{L_r + \mu h_{CG}}$$

$$^2N =$$
$$\frac{(^2F_f - {}^2F_{jy})(L_f + L_r) - k_2\varphi_2 + m_2gL_f\cos\alpha_2 + T_t - \tau A_c h_{CG}}{L_r + \mu h_{CG}}$$

$$(10)$$

where the A_c is the contact area and the joint reaction force $^2F_{jy}$ is calculated as $(k_2\varphi_2 - k_1\varphi_1)/L_c$. The resulting surface normal forces will be used to calculate the conditions of stable operation.

D. Conditions for Stable Operation

Based on the calculation of the preload and the surface normal forces, two conditions must be satisfied for stable operation of the climbing robot.

1) Positive Preload on the Front Wheels: As mentioned in Section III-B, a positive preload on the front wheel is required for the stable operation of the tread-wheel mechanism. By adjusting the compliant joint torques and the active tail forces, a positive preload condition can be satisfied. This condition is written as follows:

$$^1F_f, \quad ^2F_f \geq 0. \tag{11}$$

The effect of the compliant joint and the active tail is shown in Fig. 3. By applying the compliant torques, we can make the preload on the front wheel of the first module to be positive for every slope, which is denoted as a blue line in Fig. 3(b). The positive preload on the front wheel of the second module, as effected by the active tail force, is denoted as a cyan line in Fig. 3(d). As a result, each preload on the front wheel of each module is maintained positive regardless of the slope.

However, the rear wheel preloads are decreased as the front wheel preloads are increased by using the compliant torque and the active tail force. Due to this negative effect, the robot may detach from the surface. Therefore, there are constraints on the compliant joint force and the active tail force that are not considered in the preloads analysis. These constraints should be considered in a parametric design procedure.

2) Falling and Slipping Conditions: There are two failure conditions for a climbing robot: falling and slipping. Falling occurs when the adhesion force is not sufficient to maintain robot's weight, and slipping occurs when the friction force is not. From the free-body diagram of force conditions, as shown in
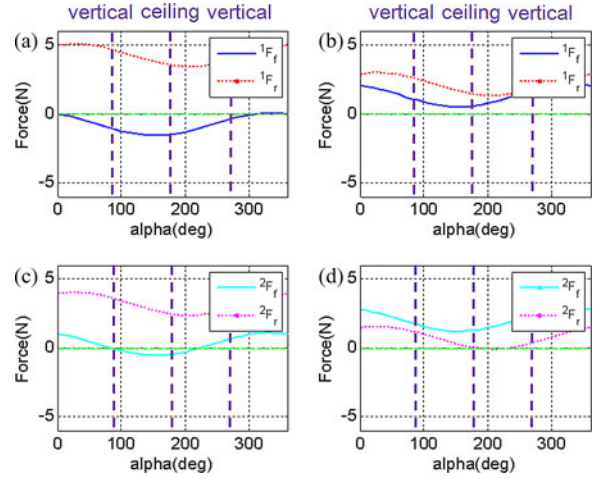

Fig. 3. Effect of the compliant joints and the active tail. Effect of the compliant joints on the first module: (a) preloads without the compliant joint force and (b) preloads with the compliant joint force. Effect of the active tail on the second module: (c) preloads without the active tail force and (d) preloads with the active tail force. Analysis is done by using parameters of $m_i = 150$ g, $L_f = L_r = 60$ mm, $L_c = 30$ mm, $h_{CG} = 15$ mm, $(k_1, k_2) = (0.06, 0.03)$ N·m/rd, $F_t = 0.7$ N, and $L_t = 150$ mm, respectively.
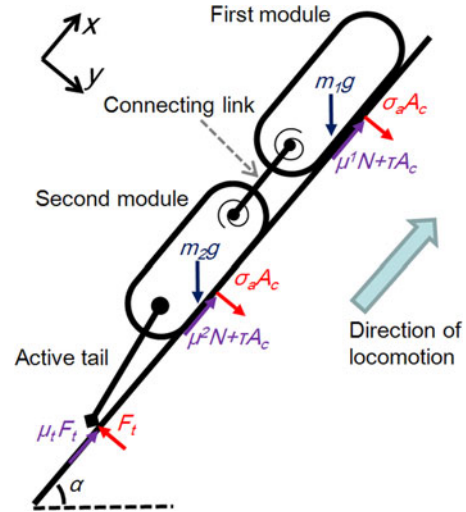

Fig. 4. Free-body diagram to calculate failure criteria. Moment equilibrium equations are derived according to tail contact position.

Fig. 4, the equilibrium equations to prevent falling and slipping are derived as follows:

$$\sum_{i=1}^{2}(\mu^iN + \tau A_c) + \mu_t F_t - Mg\sin\alpha \geq 0$$

$$2\sigma_a A_c - F_t + Mg\cos\alpha \geq 0$$

$$(\sigma_a A_c - m_1g\sin\alpha)(L_f + 2L_r + L_c + L_t)$$
$$+ (\sigma_a A_c - m_2g\sin\alpha)(L_r + L_t) - Mgh_{CG}\cos\alpha \geq 0$$

$$(12)$$

where μ_t and M denote the friction coefficient of the tail contact and total mass of the robot $(m_1 + m_2)$, respectively. α_1 and α_2 are the same α.

This article has been accepted for inclusion in a future issue of this journal. Content is final as presented, with the exception of pagination.

6   IEEE/ASME TRANSACTIONS ON MECHATRONICS

TABLE III
GEOMETRIC PARAMETERS OF THE MODULAR CLIMBING ROBOT

Parameters	L_f	L_r	L_c	L_t	w	t	r_w
Values (mm)	30	30	30	200	10	2	11

We verified these conditions by using the minimum σ_a of 2.16 kPa, and finding the resulting ^iN from (10). Note that the falling condition is critical when α is π (inverted climbing), and the slipping condition is critical when α_i is $\pi/2$ and $-\pi/2$ (vertical climbing). High F_t prevents any slipping of the robot but would cause the robot to fall; therefore, proper F_t should be determined. We can check possibility of stable climbing by selecting proper DPs, and detail procedure of parametric design is going to be introduced Section IV.

The two conditions for stable climbing can be guaranteed by selecting the proper DPs. Detailed parametric design procedure is followed in Section IV.

IV. PARAMETRIC DESIGN

A. Problem Definition

The objective of this research is to develop a fast and robust climbing robot with transitioning and obstacle overcoming abilities. DPs such as geometric lengths, compliant joint forces, and active tail forces should be determined properly to realize this objective. We can design geometric parameters such as module length or tread thickness by referring the parameters of Tankbot that clearly verified their performance in previous work [26] as shown in Table III. L_c is determined by a small value to prohibit the interference between the wheels. We have four remaining DPs to be determined: coefficients of compliant joints k_1, k_2, preloading offset joint angles φ_p, and the active tail force F_t. These parameters are very critical for robust climbing. Note that φ_p is defined as the initial angle from preloading angles of $\pi/2$ when there are no external forces on the compliant joint.

Every moving condition such as movement on a flat surface and internal/external/thin-wall transitions should be considered in the design problem. However, we can intuitively think that there are conditions such as internal and external transitions that are oppositely sensitive according to changes in the DPs. Therefore, setting up an objective function for every moving conditions does not give us a meaningful objective function for each condition. Such limitation is due to the passive compliance mechanism.

The optimization problem can be defined as follows: find four DPs $(k_1, k_2, \varphi_p, F_t)$ that maximize climbing stability on a planar surface of any slope, while the DPs guarantee working conditions for internal, external, and thin-wall transitions. The robot is expected to run mostly on a planar surface during operations, thus, optimizing the stability on a planar surface is the most reasonable choice. The other moving conditions of internal, external, and thin-wall transitions are achieved by considering them as constraints in the optimization problem. Based on this definition of the problem, the objective function and constraints can be defined. Feasibility of the problem definition is also extensively confirmed by experiments in Section V.

B. Objective Function

The objective for optimal design is to maximize stability. We have discussed two conditions in Section III related to stable operation: positive preload and preventing falling/slipping. These two conditions are related to each other as a function of preload. Since the falling condition is dominated by adhesion strength that is a function of preload as shown in (1) and slipping condition is dominated by the surface normal force, which is proportional to preload as shown in (10), we know that high preload also satisfies the falling/slipping conditions. Consequently, it is a reasonable solution to maximize the preload on the front wheels to maximize the stability of the climbing robot.

The proposed 2-D model of the modular climbing robot has two front wheels. The robot is made more stable by maximizing the average of the preloads, but deviation of the preloads should also be considered. The best design maximizes the average and minimizes the deviation of the preloads. From this point of view, we can adopt a larger-the-better signal-to-noise ratio (SNR) of the preloads as an objective function as follows [30]:

$$\text{SNR} = -10 \log \sum_{\alpha=0}^{2\pi} \left(\frac{1}{2} \sum_{i=1}^{2} \frac{1}{^iF_f^2} \right). \qquad (13)$$

The SNR is commonly used in robust design methodology. Optimization based on SNR increases both the performance and robustness of the system [30]. Therefore, we can consider the average and the deviation simultaneously using this SNR. We expect the most stable climbing along for any slope when the SNR is maximized.

It is important to note that the preloads are proportional to the stiffness coefficients and active tail force from the force analysis in Section III-B. Thus, intuitively, maximum stiffness and maximum tail force result in the maximum SNR. However, if the compliant joint torques and the active tail force are too high, these forces cause the treads to detach from the surface against the adhesion force, resulting in a folded body shape. Hence, the definition of constraints is very important to limit the range of the DPs, and optimum values are expected to be determined at a boundary of the inequality constraints. Detailed constraints are derived in Section IV-C.

C. Constraints

As mentioned in Section IV-B, definition of the constraints is very important in parametric design for this robot configuration since the solution is expected to be determined at a boundary of the constraints. Among the four DPs, three DPs related to the compliant joints(k_1, k_2, φ_p) are constrained by conditions during flat surface climbing and internal transition. The active tail force F_t is optimized independently for each condition of flat, internal, and external transition. Three equations of falling and slipping conditions in (12) are also included as constraints for stable climbing.

1) Flat Surface Climbing and Internal Transition: During flat surface locomotion and the internal transition, the robot

This article has been accepted for inclusion in a future issue of this journal. Content is final as presented, with the exception of pagination.

SEO AND SITTI: TANK-LIKE MODULE-BASED CLIMBING ROBOT USING PASSIVE COMPLIANT JOINTS
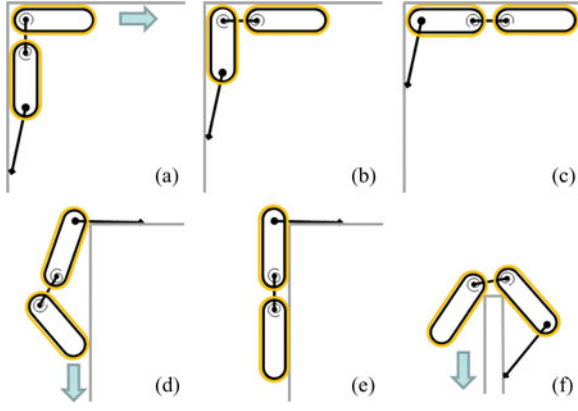
7

Fig. 5. Setup to calculate static constraints: (a)–(c) during internal transition, (d)–(e) external transition, and (f) thin-wall transition.

must satisfy (14) to maintain adhesion on the surface:

$$(\sigma_a A_c + m_i g \cos \alpha_i) L_f + m_i g h_{CG} \sin \alpha_i + {}^i F_r (L_f + L_r) \geq 0 \tag{14}$$

where $i = 1, 2$. These equations are derived from the moment equilibrium condition of each module. Since the robot is expected to detach from the rear wheel, which means that the compliant torque and the active tail force are too high, so the moment equilibrium equation (14) is calculated according to the contact point of each front wheel. By satisfying these equations, the tread can maintain adhesion against the negative effects of the compliant joints and the active tail. Since these equations are derived for each module, the equations can be applied in the internal transitions.

During an internal transition, the compliant joints are rotated in opposing directions, and high compliance torques are generated between modules. These compliant torques could cause the modules to detach from the surface if the compliant torques are too high. This failure mode can be avoided by satisfying (14), while the preload due to the compliant joints and the active tail are changed according to external conditions.

The conditions for internal transition can be classified for three extreme configurations. The postures are shown in Fig. 5(a)–(c). We checked that the conditions between the three configurations in Fig. 5(a)–(c) are guaranteed if three conditions are satisfied. Thus, these three conditions are considered as constraint equations. Note that after the first module transition (a), only ${}^1 F_{cr}$ term is changed while the other terms are the same as for flat surface climbing. In the posture of (b), ${}^2 F_{cf}$ term is changed while the other terms stay the same. After two modules have transitioned (c), ${}^2 F_{tr}$ term is changed from flat surface climbing. During the internal transition, one of the tread is assumed to be detached from the surface. Detailed equations as changed from (8) and (9) are derived as follows:

For case (a):

$$^1 F_{cr} = -\frac{k_1 \varphi_1}{L_f + L_r} \tag{15}$$

for case (b):

$$^2 F_{cf} = -\frac{k_2 \varphi_2}{L_f + L_r} \tag{16}$$

for case (c):

$$^2 F_{tr} = -F_t \left(\mu_t + \frac{L_t}{L_f + L_r} \right). \tag{17}$$

Note that the φ_i terms are changed according to each conditions. Calculated preloads from these equations are used in (14) to give us an upper limit for the compliant joint forces and the active tail force.

There is a regime in which the compliant torque lifts the body of the second module between Fig. 5(b) and (c). The conditions leading to this regime can be expressed as follows:

$$\frac{k_1 \varphi_1 - k_2 \varphi_2}{L_c} + m_2 g \cos \alpha_2 > 0. \tag{18}$$

This equation give us the lower limit for the compliant joint forces during an internal transition.

2) External and Thin-Wall Transition: Two relatively simple transitions are considered: vertical to horizontal, horizontal to vertical external transitions, and vertical to inverse-vertical thin-wall transition. These external/thin-wall transitions should be autonomously performed using the compliant torques and the active tail force. During the vertical to horizontal external transition, only the stiffness coefficients of each joints and the active tail force are required to be positive since the modules are supported by the horizontal surface after transitioning.

During the horizontal to vertical transition and thin-wall transition, the active tail plays an important role. Once the two modules have completed the transition, the active tail supports the entire body mass before the treads of each modules make full contact with the vertical surface as shown in Fig. 5(d). At this point, the peeling of each tread propagates on to the vertical surface while the active tail supports the body mass. Once both treads are fully in contact on the vertical surface as shown in the Fig. 5(e), the robot resumes motion. During the thin-wall transition, the procedure of transitioning is exactly the same with the horizontal to vertical external transition. To achieve this transition, the compliant joints and the active tail force should be determined to satisfy these equations:

$$k_i > 0, \quad i = 1, 2$$
$$F_t L_t - M g r_w \geq 0 \tag{19}$$
$$(Mg + 2\tau A_c) r_w - F_t L_t \geq 0$$

where the $2\tau A_c$ term is the minimum friction force of V-10 tread on the surface from (2). Note that the (19) requires the torque induced by the active tail to be larger than the mass of the robot and smaller than the summation of the mass of the robot and the friction of the treads.

In addition, geometric constraints of the thin-wall thickness that can be overcome by the robot are defined from Fig. 5(f) as follows:

$$t_w > L_c - 2 r_w \tag{20}$$

This article has been accepted for inclusion in a future issue of this journal. Content is final as presented, with the exception of pagination.

8   IEEE/ASME TRANSACTIONS ON MECHATRONICS

TABLE IV
RESULTING OPTIMAL DPS

Parameters (Units)	k_1 ($N \cdot m/rad$)	k_2 ($N \cdot m/rad$)	φ_p (rad)	F_t (N)
flat/internal external	0.0225	0.005	$\pi/4$	0.677 0.140

where t_w is the thickness of the thin-wall that is set to 8 mm, as given in Table III. This constraint is from the condition that the two wheels should contact the edges of the thin-wall simultaneously.

D. Results

The design problem for determining the four DPs is solved to maximize the objective function under the suggested constraints. MATLAB functions are used to numerically solve the problem. Before solving the problem, note that the objective function is proportional or inversely proportional to each DP from (8) and (9); therefore, we expect the optimal values would be determined at the boundary of the constraints. φ_p and (k_1, k_2) are correlated with determine the preloads; so, we need to have an assumption on one of those parameters. Therefore, we set φ_p to be fixed as $\pi/4$ to determine a unique solution by ignoring the coupling between the stiffness coefficients and φ_p.

As expected, the resulting DPs are at the boundary of the constraint inequalities since the DPs have a proportional relation to the objective function. Actually, k_2 is calculated as a small positive number that is at the boundary of (19). And so k_2 is determined as 0.005 N·m/rd, which is the minimum positive value that can be realized by the compliant joint as designed. Note the k_2 is calculated by small positive number in the optimal design problem. The four resulting DPs are shown in Table IV. Based on this result, we selected (k_1, k_2, φ) as (0.02 N·m/rd, 0.005 N·m/rd, $\pi/4$) in the design of the prototype. The active tail force is varied according to the robot's moving condition (0.677 N in flat surface climbing or internal transitioning, and 0.140 N during external transitioning). These DPs allow the climbing robot to perform flat surface climbing as well as internal, external, and thin-wall transitions, which are presented in Section V.

V. EXPERIMENTAL RESULTS AND DISCUSSION

A. Prototype Description

The developed prototype is shown in Fig. 6. The robot is 180 mm (length) × 180 mm (width) × 50 mm (height) excluding the active tail and 180 g weight including the V-10 treads [first module (68 g) and second module (112 g)]. The acrylic frames are manufactured by a laser cutter (Venus), and the wheels are made by a 3-D printer (3-D Systems Invision HR). All parts are bonded by a super glue. Compliant torques are achieved using rubber bands around a cylindrical Delrin rod in the joints, as shown in Fig. 7. The extension of each rubber band determines the compliant torque, and it is changed passively according to the slope of the surface α_i. The compliant torques are calibrated experimentally. The active tail is operated by adopting a proportional controller using feedback signal from a force sensor.
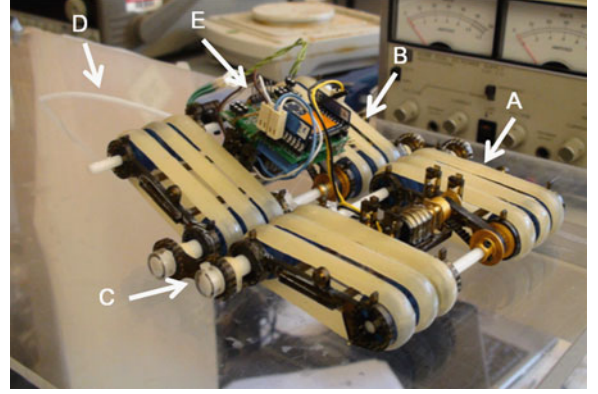

Fig. 6. Prototype of the modular climbing robot: A denotes the first module; B denotes the second module; C denotes the connecting link; D denotes the active tail; and E denotes the microcontroller.
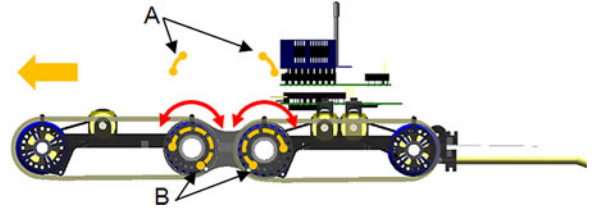

Fig. 7. Rubber mechanism for compliance torque (red lines): A denotes the initial rubber band length; B denotes the rubber band during flat surface climbing with pretension.

A PIC microcontroller (PIC18F4620, Microchip) is used with commercial motor drivers (microdual serial motor controller, Pololu) to operate actuators (298 : 1 Mini metal gear motor, Solarbotics).

It is important to note that contamination of the dry adhesives treads degrades the adhesive force by time. Many researchers have been working on the self-cleaning ability of the dry adhesives [12], [14]; however, there is no satisfactory solution yet. In this study, the V-10 tread is cleaned by ethyl alcohol each time before experiments to prevent any contamination.

B. Climbing on a Flat Surface

The assembled prototype is tested on various surfaces. The robot can climb a slope of 0° to 360° on smooth surfaces such as acrylic and glass. Moreover, the robot can locomote vertically on relatively rough surfaces such as brick, steel, and wood. The robot shows high speed vertical climbing of 6 cm/s on acrylic surface. A payload capacity of 500 g is also successfully verified (see Multimedia Extension 1, Windows Media Video, Supplementary Material at http://ieeexplore.ieee.org).

Fig. 8 shows the effect of force transfer due to the peeling force and the compliant torque. The robot is initially configured as in Fig. 8(a) because of differences between the two compliant joint forces. After moving the two wheels forward, the robot passively changes into a flat configuration as in Fig. 8(b)–(f) since the adhesion and the peeling forces are dominant. After changing to the flat configuration, the force analysis results in Section III can be used to determine the preloads and the surface normal forces.
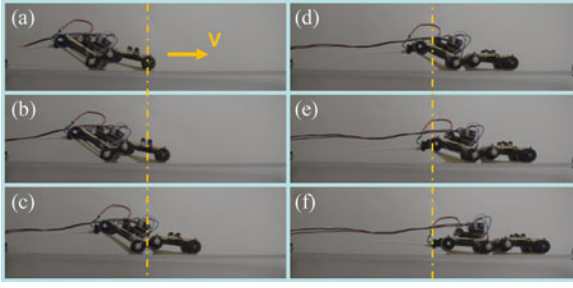
Fig. 8. Photo snapshot of force transfer due to the peeling/adhesion forces and the compliant torque: (a) Initial configuration. (b) Robot starts moving. (c) Adhesion and peeling forces pull the first module toward the surface against the compliant torque. (d) Adhesion and peeling forces pull the second module toward the surface against the active tail force (e) and (f) Robot is running in a flat configuration.
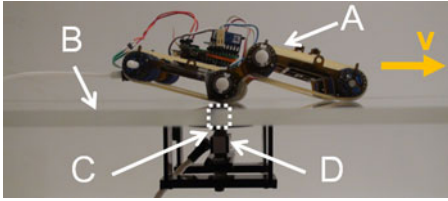

Fig. 9. Preload measurement setup: A denotes the robot; B denotes the acrylic plate; C denotes slit that is connected to the load cell; D denotes the load cell.

Fig. 10. Experimental preload data of horizontal surface locomotion: (a) forces with small stiffness coefficients [$(k_1, k_2) = (0.01, 0.005)$ N·m/rd]; (b) forces with high stiffness coefficients ((k_1, k_2)=(0.02, 0.005) N·m/rd); and (c) forces with high stiffness coefficients with the active tail force ((k_1, k_2) = (0.02, 0.005) N·m/rd), $F_t = 0.32$ N, (A: ^1F_f, B: ^1F_r, C: $^1F_{rp}$, D: ^2F_f, E: ^2F_r, F: $^2F_{rp}$).

To verify the effects of the compliant joint force and the active tail force on the preloads of the wheels, as calculated in Section III-B, we built a force measurement setup using a load cell (Transducer Techniques, MLP-10) on a acrylic surface. Detailed measurement setup is shown in Fig. 9. On a flat acrylic surface, we cut a slit of 3×200 mm^2 for the measurement. The slit is filled with 3×200 mm^2-sized long piece of acryl, and the acryl piece is connected to the load cell below. Using this setup, we measured preloads on horizontal running and on vertical climbing. While the robot passed the slit, the static force of each part was measured by the load cell sequentially. Since the experiments aim to prove the static calculation results on preloads, the robot is operated relatively slowly (1 cm/s) in order to minimize dynamic effects.

Measured data from climbing on a horizontal and vertical surface are shown in Fig. 10. When the robot reaches the force sensitive area, the front and rear wheel (^1F_f, ^1F_r) of the first module run over the sensor. After that, the peeling force $^1F_{pr}$ is measured where the tread is detached. This sequence is repeated when the second module ^2F_f, ^2F_r, $^2F_{pr}$ runs over the sensor, and finally the tail runs over the sensor. Note that as higher k_1 is applied, ^1F_f, ^2F_f, ^2F_r are increased while ^1F_r is decreased. After applying the active tail force, ^2F_r is transferred to ^2F_f as expected.

Simulation and experimental results are compared in Fig. 11. Fig. 11(a)–(b) shows results from the horizontal surface and Fig. 11(c)–(d) shows results from the vertical surface. As expected, high compliant torques positively affect the front wheels of the first and the second module. The tail force only increases the preload on the front wheel of the second module. Even though there is a relatively large error in the result of the ver-
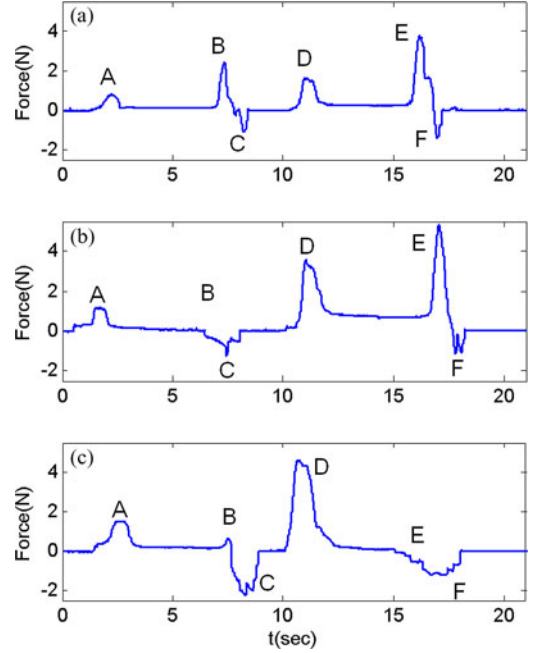
tical surface experiment, the trend of measured preloads are coincident to the simulation. We believe these errors are mainly due to alignment error between the left and right wheels.

We note the limited performance on ceiling. If we do not drive the robot on ceiling continuously, the robot falls after a short time since the compliance torques of the joints generate negative torque to peel off the tread. Note the compliant joints are designed based on the forward driving condition. Adopting active compliant joints would be helpful for staying statically for long durations, as proposed by [26].

C. Transitions and Obstacles

One of the most important objectives of the proposed robot is to achieve dexterous motions. In this section, the performance during internal, external, and thin-wall transitioning and obstacle overcoming is presented.

1) Internal Transitions: The modular climbing robot is tested on three possible internal transitions to validate the locomotion scenario. Compliant joint parameters and active tail forces are set based on the optimal design result in Section IV. As a result, capabilities of performing three internal transitions are successfully verified.

Three internal transitions were empirically possible excluding vertical to ceiling transition. The detailed posture during the internal transition are shown in Fig. 12(a)–(d) (See also Multimedia Extension 1). Note that after the first module complete the transition, the second module pushes the connecting links toward the wall. During this step, the speed of the second module

This article has been accepted for inclusion in a future issue of this journal. Content is final as presented, with the exception of pagination.

10   IEEE/ASME TRANSACTIONS ON MECHATRONICS
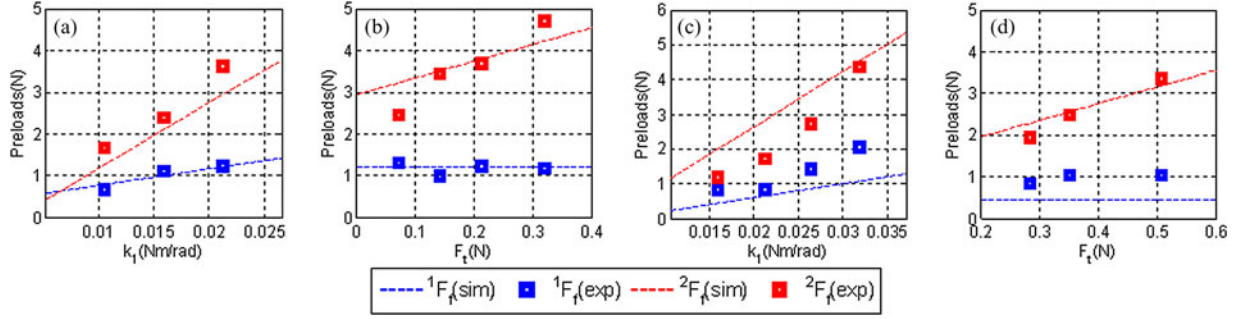

Fig. 11. Comparison of simulation and experimental data on (a) and (b) horizontal surface and (c) and (d) vertical surface. (a) Preloads according to compliant torques without an active tail (k_2 is fixed as 0.005 N·m/rd). (b) Preloads according to active tail force (k_1 and k_2 are fixed as 0.02 N·m/rd and 0.005 N·m/rd). (c) Preloads according to the compliant joint on the vertical surface (k_2 and F_t are fixed as 0.005 N·m/rd and 0.21 N). (d) Preloads according to the active tail force (k_1 and k_2 are fixed as 0.015 N·m/rd and 0.005 N·m/rd).
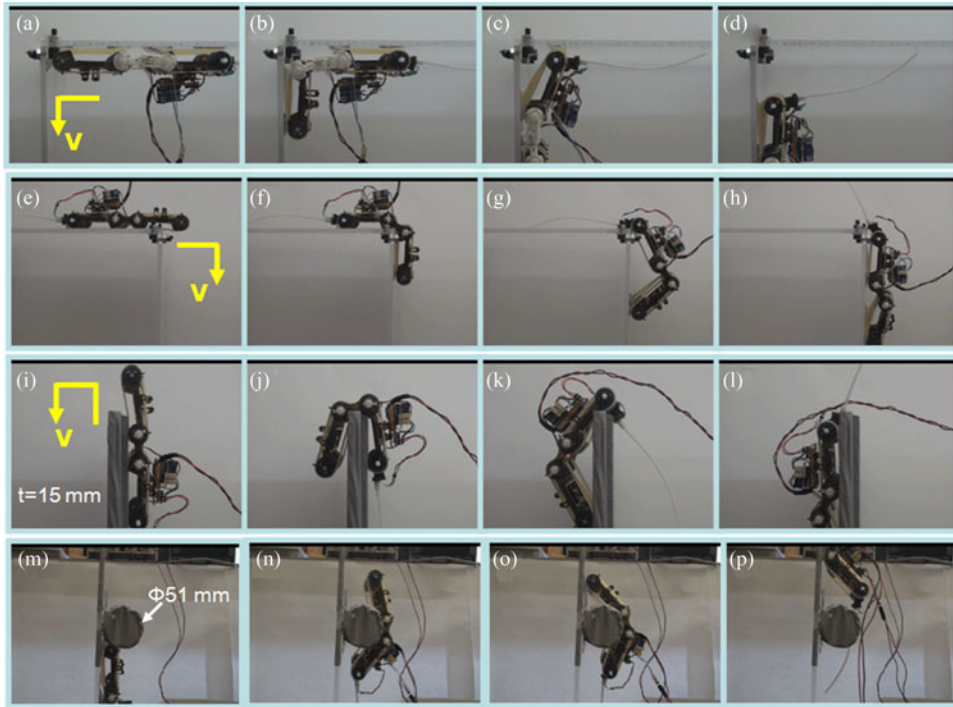

Fig. 12. Photograph snapshots during experiments (see Multimedia Extension 1). Internal transition. (a) Front wheel touches the wall. (b) First module finishes transition. (c) Second module is transitioning. (d) Robot finishes transitioning. External and thin-wall transition: (e) and (i) First module starts transitioning. (f) and (j) First module touches the surface to be transitioned. (g) and (k) Second module is transitioning while the active tail supports the body. (h) and (l) Tread friction makes the robot run forward. 51-mm obstacle overcoming: (m) First module touches the obstacle. (n) Robot rolls around the obstacle. (o) Front wheel of the first module contacts the wall while the active tail cancels pitch-back moment; (p) Transition is completed.

is increased to enable the front wheel of the second module to contact with the wall. Then, the second module completes the transition with peeling propagation and the active tail follows.

Although we checked the possibility of transitioning through the static force equation of adhesion force and preload in Section IV, one remaining vertical to ceiling transition was not achieved with the compliant underactuated robot. After the second module finishes the transition, the compliant joint module must lift up the whole body against gravity, causing the tread to attach to the surface. The inequality equation for the compliant torque must be satisfied to accomplish the vertical to ceiling transition as follows:

$$k_2\varphi_2 - m_2gL_f > 0. \tag{21}$$

This equation gives us a lower bound of $k_2 > 0.014$ N·m/rd. However, large k_2 decrease the preload on the front wheels as shown in (9). If we design robot to satisfy this equation, the other constraint equations cannot be satisfied simultaneously, since there is conflict between the constraints. This results in the robot being unable to perform even flat surface climbing. Since the compliant joint force is not sufficient to lift up the body, the robot falls during the transition. Consequently, vertical to ceiling transition is not accomplished using the underactuated climbing robot, and is a limitation of the robot.

2) External and Thin-Wall Transitions: External transition capability is tested, and two external transitions of vertical to horizontal and horizontal to vertical directions are achieved.

The detailed posture of these transitions were presented in Multimedia Extension 1. The vertical to horizontal transition is performed naturally via the inward compliant and active tail forces. The tail follows after the transition since the inertia and friction forces of the robot are higher than the active tail force.

A horizontal to vertical transition and thin-wall transitions of up to 15 mm thick were achieved through a similar procedure (see Fig. 12 (e)–(l)]. After both modules are transitioned, they detach from the surface. Then the active tail supports the whole body while the peelings of the treads propagate onto the surface as expected in (19). After that, the robot can move forward since the summation of the friction and the gravity forces are higher than the active tail force.

There are two more external transitions besides the thin-wall transition: vertical to ceiling and ceiling to vertical. The compliant torques must be sufficient to lift up the first module during these transitions. We can derive the force equation for the second compliant torques for these transitions as follows:

$$k_2 \varphi_2 - m_1 g(L_r + L_c) > 0 \tag{22}$$

where φ_2 is φ_p in vertical to ceiling transition and $\pi/2 + \varphi_p$ in the ceiling to vertical transition to give us constraints of $k_2 > 0.051$ N·m/rd and $k_2 > 0.017$ N·m/rd, respectively. These constraints cannot be satisfied simultaneously with the constraints in Section IV. Thus, there is no unique solution for the proposed robot design to perform every external transition.

Additionally, we consider several explanations for the limited external and thin-wall transitioning capability such as mechanical interferences during transitions and limited adhesion forces to prevent falling and slipping. We think these transitions could be done by designing a new modular robot using precisely controlled active compliant joints and using an adhesion material with improved adhesion forces, such as those using fibrillar adhesives. More modules could also be solution for this. Consequently, external transitions in extreme conditions remain as a limitation of the proposed underactuated modular climbing robot.

3) Overcoming Obstacles: The capability to overcome various obstacles are investigated. Even though a theoretical ability to overcome obstacles is not specifically analyzed, we can intuitively expect this ability since overcoming of obstacles is considered as a combination of internal and external transitions. Detailed 51-mm obstacle overcoming snapshots are shown in Fig. 12(m)–(p) (also see Multimedia Extension 1). It is important to note that when the second module is totally detached from the flat surface during large obstacle overcoming, the active tail is very important to cancel the pitch-back moment. Longer L_c could be helpful to increase stability in the obstacle overcoming; however, there is also limitation of L_c due to thin-wall transition in (20). Empirically, the robot can overcome up to 51-mm sized obstacle that is similar to the length of a single module $(L_f + L_r)$ of 60 mm. We believe the limitation is due to the limited compliance of the second module as internal transition case in (21). In conclusion, the robot can overcome obstacles of size up to that of a single module.

4) Summary on Internal/External Transitions: We summarized the on transitioning capability of the proposed robot in
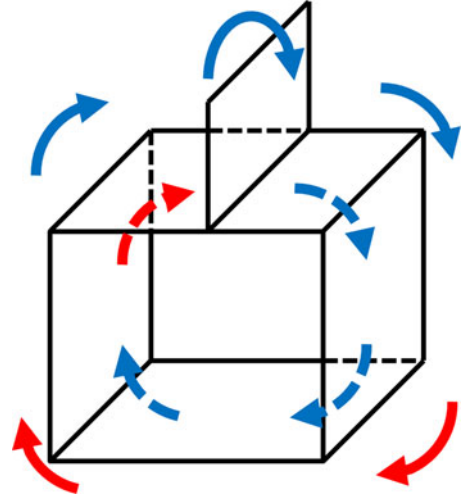

Fig. 13. Transitioning capability of the proposed robot. Solid lines denote external transitions including thin-wall transition and dashed lines show internal transitions.

Fig. 13. Blue lines denote the possible transitions and red lines denote the impossible transitions by the proposed climbing robot. The failed transitions are mainly due to the limitation of passive compliances of the robot. As we discussed before, a new robotic platform using more modules with active compliance would remove these limitations as a future work.

VI. CONCLUSION

Analysis, prototype, and experiments of a modular climbing robot with dry elastomer treads were presented in this paper. The proposed design requirement of high speed climbing is satisfied by using a wheeled mechanism design with V-10 flat elastomer adhesive treads and the ability to perform three internal, two external, one thin-wall transitioning, and overcoming various sized obstacles are satisfied by a combination of compliant joints and an active tail. The compliant joints and the active tail work to increase stability for flat surface locomotion and adaptability for various moving conditions. Optimal DPs are determined based on the force analysis to maximize stability during flat surface climbing while versatility for various transitions are guaranteed. The assembled prototype is validated through experiments in various moving conditions.

The concept of joint compliance could be adopted in other climbing robots to enhance stability. The compliant torques can be optimally controlled using the active joint modules, while robots requiring the use of a feedback controller with sensors. Even though stable operation of the proposed modular climbing robot is verified in various moving conditions, there are several remaining problems to be solved for applications in a real environment. The remaining transitions such as the vertical to ceiling transition must be achieved increasing the number of robot modules while decreasing their size. Preventing contamination of the elastomer adhesives and locomotion on a 3-D surfaces are also candidates for future work.

REFERENCES

[1] T. Bretl, "Motion planning of multi-limbed robots subject to equilibrium constraints: The free-climbing robot problem," *Int. J. Robot. Res.*, vol. 25, no. 4, pp. 317–342, 2006.

[2] W. R. Provancher, S. I. Jensen-Segal, and M. A. Fehlberg, "ROCR: An energy-efficient dynamic wall-climbing robot," *IEEE/ASME Tran. Mechatronics*, vol. 16, no. 5, pp. 895–906, Oct. 2011.

[3] Y. K. Song, C. M. Lee, I. M. Koo, D. T. Tran, H. Moon, and H. R. Choi, "Development of wall climbing robotic system for inspection purpose," in *Proc. IEEE/RSJ Int. Conf. Intell. Robots Syst.*, Nice, France, 2008, pp. 1990–1995.

[4] H. Zhang, J. Zhang, G. Zong, W. Wang, and R. Liu, "Sky Cleaner 3: A real pneumatic climbing robot for glass-wall cleaning," *IEEE Robt. Autom. Mag.*, vol. 13, no. 1, pp. 32–41, Mar. 2006.

[5] J. Xiao, A. Sadegh, M. Elliot, A. Calle, A. Persad, and H. M. Chiu, "Design of mobile robots with wall climbing capability," in *Proc. IEEE/ASME Int. Conf. Adv. Intell. Mechatron.*, Monterey, CA, 2005, pp. 438–443.

[6] W. Fischer, G. Caprari, R. Siegwart, and R. Moser, "Compact magnetic wheeled robot for inspecting complex shaped structures in generator housings and similar environments," in *Proc. IEEE/RSJ Int. Conf. Intell. Robots Syst.*, St. Louis, MO, 2009, pp. 4116–4121.

[7] G. C. Haynes, A. Khripin, G. Lynch, J. Amory, A. Saunders, A. A. Rizzi, and D. E. Koditschek, "Rapid pole climbing with a quadrupedal robot," in *Proc. IEEE Int. Conf. Robot. Autom.*, Kobe, Japan, 2009, pp. 2767–2772.

[8] D. Longo and G. Muscato, "The Alicia³ climbing robot: A three-module robot for automatic wall inspection," *IEEE Robot. Autom. Mag.*, vol. 13, no. 1, pp. 42–50, Mar. 2006.

[9] H. Prahlad, R. Pelrine, S. Stanford, J. Marlow, and R. Kornbluh, "Electroadhesive robots-wall climbing robots enabled by a novel, robust, and electrically controllable adhesion technology," in *Proc. IEEE Int. Conf. Robot. Autom.*, Pasadena, CA, 2008, pp. 3028–3033.

[10] M. Murphy and M. Sitti, "Waalbot: An agile small-scale wall-climbing robot utilizing dry elastomer adhesives," *IEEE/ASME Trans. Mechatronics*, vol. 12, no. 3, pp. 330–338, Jun. 2007.

[11] O. Unver and M. Sitti, "Flat dry elastomer adhesives as attachment materials for climbing robots," *IEEE Trans. Robot.*, vol. 26, no. 1, pp. 131–141, Feb. 2010.

[12] J. Lee and R. S. Fearing, "Contact self-cleaning of synthetic gecko adhesive from polymer microfibers," *Langmuir*, vol. 24, no. 19, pp. 10587–10591, 2008.

[13] S. Floyd and M. Sitti, "Design and development of the lifting and propulsion mechanism for a biologically inspired water runner robot," *IEEE Trans. Robot.*, vol. 24, no. 3, pp. 698–709, Jun. 2008.

[14] S. Kim, M. Spenko, S. Trujillo, B. Heyneman, D. Santos, and M. R. Cutkosky, "Smooth vertical surface climbing with directional adhesive," *IEEE Trans. Robot.*, vol. 24, no. 1, pp. 65–74, Feb. 2008.

[15] K. Daltorio, T. E. Wei, A. D. Horchler, L. Southard, G. D. Wile, R. D. Quinn, S. N. Gord, and R. E. Ritzmann, "Mini-Whegs^{TM} climbs steep surfaces using insect-inspired attachment mechanism," *Int. J. Robot. Res.*, vol. 28, no. 2, pp. 285–302, 2009.

[16] M. P. Murphy, C. Kute, Y. Menguc, and M. Sitti, "Waalbot II: Adhesion recovery and improved performance of a climbing robot using fibrillar adhesives," *Int. J. Robot. Res.*, vol. 30, no. 1, pp. 118–133, 2011.

[17] O. Unver and M. Sitti, "Tankbot: A palm-size, tank-like climbing robot using soft elastomer adhesive treads," *Int. J. Robot. Res.*, vol. 29, no. 14, pp. 1761–1777, 2010.

[18] O. Unver and M. Sitti, "Tankbot: A miniature, peeling based climber on rough and smooth surrfaces," in *Proc. IEEE Int. Conf. Robot. Autom.*, Kobe, Japan, 2009, pp. 2282–2287.

[19] J. Guo, K.-M. Lee, D. Zhu, X. Yi, and Y. Wang, "Large-deformation analysis and experimental validation of a flexure-based mobile sensor node," *IEEE/ASME Trans. Mechatronics*, vol. PP, no. 99, pp. 1–11, Mar. 2011.

[20] P. Birkmeyers, K. Peterson, and R. S. Fearing, "DASH: A dynamic 16g hexapedal robot," in *Proc. IEEE/RSJ Int. Conf. Intell. Robots Syst.*, St. Louis, MO, 2009, pp. 2683–2689.

[21] A. T. Asbeck, S. Kim, M. R. Cutkosky, W. R. Provancher, and M. Lanzetta, "Scaling hard vertical surfaces with compliant microspine arrays," *Int. J. Robot. Res.*, vol. 25, no. 12, pp. 1165–1179, 2006.

[22] H. Wei, Y. Chen, J. Tan, and T. Wang, "Sambot: A self-assembly modular robot system," *IEEE/ASME Trans. Mechatronics*, vol. 16, no. 4, pp. 745–757, Aug. 2011.

[23] J. Xiao, A. Calle, A. Sadegh, and M. Elliot, "Modular wall climbing robots with transition capability," in *Proc. IEEE Int. Conf. Robot. Biomimet.*, Hong Kong, China, pp. 246–250.

[24] Y. Liu and G. Liu, "Track-stair interaction analysis and online tipover prediction for a self-reconfigurable tracked mobile robot climbing stairs," *IEEE/ASME Trans. Mechatronics*, vol. 14, no. 5, pp. 528–538, Oct. 2009.

[25] J. Y. Wong, *Theory of Ground Vehicles*. New York: Wiley, 2008.

[26] O. Unver and M. Sitti, "A miniature ceiling walking robot with flat tacky elastomeric footpads," in *Proc. IEEE Int. Conf. Robot. Autom.*, Kobe, Japan, 2009, pp. 2276–2281.

[27] T. Tang, C. Y. Hui, and N. J. Glassmaker, "Can a fibrillar interface be stronger and tougher than a non-fibrillar one?" *J. R. Soc. Interface*, vol. 2, pp. 505–516, 2005.

[28] E. Meyer, R. M. Overney, K. Dransfeld, and T. Gyalog, *Nanoscience: Friction and Rheology on the Nanometer Scale*. Singapore: World Scientific, 1998.

[29] K. Kendal, "Thin-film peeling-the elastic term," *J. Phys. D, Appl. Phys.*, vol. 8, pp. 1949–1952, 1975.

[30] G. Taguchi, *Taguchi on Robust Technology Development: Bringing Quality Engineering Upstream*. New York: ASME, 1993.

TaeWon Seo (M'10) received the B.S. and Ph.D. degrees from the School of Mechanical and Aerospace Engineering, Seoul National University (SNU), Seoul, Korea, in 2003 and 2008, respectively.

He is currently a Faculty Member in the School of Mechanical Engineering, Yeungnam University, Gyeongsan, Korea. During 2008–2009, he was a Researcher with the Institute of Advanced Machinery and Design, SNU. During 2009–2010, he was a Postdoctoral Research Associate in the NanoRobotics Laboratory, Carnegie Mellon University. His current research interests include mechanism design, optimal design, control, and motion planning of robotic systems.

Metin Sitti (S'94–M'00–SM'08) received the B.Sc. and M.Sc. degrees in electrical and electronics engineering from Bogazici University, Istanbul, Turkey, in 1992 and 1994, respectively, and the Ph.D. degree in electrical engineering from The University of Tokyo, Tokyo, Japan, in 1999.

During 1999–2002, he was a Research Scientist at the University of California at Berkeley. He is currently a Professor in the Department of Mechanical Engineering and Robotics Institute, Carnegie Mellon University, Pittsburgh, PA. He is also the Director of the NanoRobotics Laboratory and the Center for Bio-Robotics. His research interests include micro/nanorobotics, bioinspired materials and miniature mobile robots, and micro/nanomanipulation.

Dr. Sitti received the SPIE Nanoengineering Pioneer Award in 2011. He was appointed as the Adamson Career Faculty Fellow during 2007–2010. He was the Vice-President for Technical Activities of the IEEE Nanotechnology Council during 2008–2010. He was elected as a Distinguished Lecturer of the IEEE Robotics and Automation Society for 2006–2008. He received a National Science Foundation CAREER Award and the Struminger Award in 2005. He received the Best Paper Award at the IEEE/RSJ International Conference on Intelligent Robots and Systems in 2009 and 1998, the second prize at the World RoboCup Nanogram Demonstration League in 2007, the Best Biomimetics Paper Award at the IEEE Robotics and Biomimetics Conference in 2004, and the Best Video Award at the IEEE Robotics and Automation Conference in 2002. He is the Co-Editor-In-Chief of the *Journal of Micro/Nano-Mechatronics* and an Associate Editor of the IEEE TRANSACTIONS ON ROBOTICS and *ACS Applied Materials and Interfaces*.